Progress Survey of X-Ray Refraction Imaging Techniques

Andreas KUPSCH [1], Bernd R. MÜLLER [1], Manfred P. HENTSCHEL [2], Axel LANGE [1], Volker TRAPPE [1], René LAQUAI [1], Yury SHASHEV [1], Sergei EVSEVLEEV [1,3,4], Giovanni BRUNO [1,5]

[1] BAM Bundesanstalt für Materialforschung und -prüfung, 12200 Berlin, Germany,
[2] Technical University Berlin, Polymertechnik / Polymerphysik, 10587 Berlin, Germany,
[3] Dresden International University, Freiberger Str. 37, 01067 Dresden, Germany,
[4] Tomsk Polytechnic University, Institute of NDT, Tomsk, 634050, Russia,
[5] University Potsdam, Institute of Physics and Astronomy, 14476 Potsdam-Golm, Germany

Contact e-mail: andreas.kupsch@bam.de

Abstract. The most substantial innovations in radiographic imaging techniques of the last two decades aim at enhanced image contrast of weakly absorbing micro and nano structures by taking advantage of X-ray refraction effects occurring at outer and inner surfaces. The applications range from fibre reinforced plastics to biological tissues.

These techniques comprise, among others, X-ray refraction topography, diffraction enhanced imaging, phase contrast imaging, Talbot-Lau grating interferometry, and refraction enhanced imaging. They all make use of selective beam deflections up to a few minutes of arc: the X-ray refraction effect. In contrast to diffraction, this type of interaction has a 100 % scattering cross section, as shown experimentally. Since X-ray refraction is very sensitive to the orientation of interfaces, it is additionally a tool to detect, *e.g.*, fibre or pore orientation. If the detector resolution exceeds the size of (small) individual features, one detects the integral information (of inner surfaces) within the gauge volume.

We describe the above-mentioned techniques, and show their experimental implementation in the lab and at a synchrotron source. We also show strategies for data processing and quantitative analysis.

Introduction

The prevailing common sense of X-ray imaging is dominated by medical applications, purely taking advantage of the different absorption behaviour of different material. Even in the numerous branches of engineering, absorption is the only one interaction utilized (or considered, respectively). Mostly, scattering effects are unwanted in radiological applications, since they distort the primary beam intensity. Together with beam hardening they are empirically combined to a so-called build-up factor, which is used for rough intensity correction.

However, all kinds of X-ray scattering such as (elastic) diffraction, (inelastic) Compton scattering, or X-ray fluorescence can be employed for imaging techniques, given a suited discrimination of primary radiation. This can be achieved by either pure geometric restrictions (by collimation) or by scattering specifications. As a result, one obtains 2D distributions ("images"), which depict the desired interaction parameter.

It should be noted, that, in contrast to the established NDT techniques, scattering imaging is not focused on obtaining individual flaws or indications but on the determination of microstructural parameters (relevant for material properties). The constituent elements of such microstructures may be much smaller than the image resolution as they create signals by any kind of scattering interaction. The lower limit of structure sizes is simply given by the X-ray wavelength (usually of atomic dimension).

Driven by partly insufficient performance of conventional techniques in case of hidden interface microstructures of relevance for material properties, we focus on imaging techniques based on X-ray refraction. Refractive X-ray deflection occurs, when X-rays interact with interfaces (cracks, pores, particles, phase boundaries) similar to visible light in transparent materials (lenses or prisms). However, X-ray optical effects can be observed only at small scattering angles between several seconds and a few minutes of arc as the refractive index n of X-rays is nearly unity. Let δ be the real part of the complex index of refraction index n, ρ the electron density and λ the X-ray wavelength, then is $n = 1 - \delta$, with $\delta \approx \rho \cdot \lambda^2$ (*e.g.*, $\delta \approx 10^{-6}$ for glass at 20 keV radiation), neglecting the imaginary part β, which counts for absorption. Since Snell's law (of refraction) holds for X-rays as well, this implies, that the incident angle of X-rays relative to the surface should be small enough in order to achieve a measurable deflection angle.

1. A selection of X-ray refraction techniques

In the course of progress in X-ray sources, computing power, detector resolution and dynamics various techniques to create high contrast refraction images have developed into mature methods for systematic micro structure investigations. Table 1 presents the basic principles by sketches of their typical beam geometries. Table 2 lists their discrimination terms and essential scanning dimensions.

Due to the short X-ray wavelength, X-ray refraction techniques are able to detect the scattering response of nano structures without imaging the individual interfaces.

Table 1. List of schematics of X-ray refraction techniques.

Technique	Scheme
Pinhole Topography	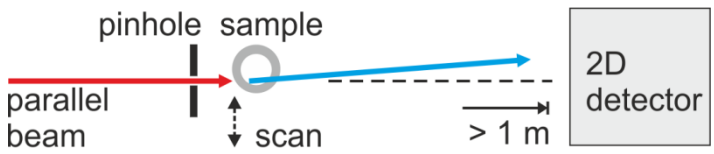
Refraction Topography	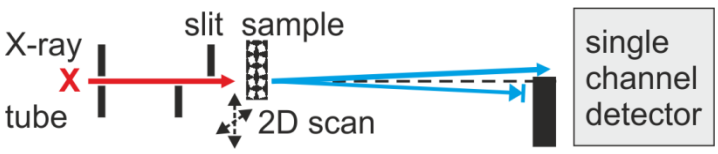
Phase Contrast Radiography	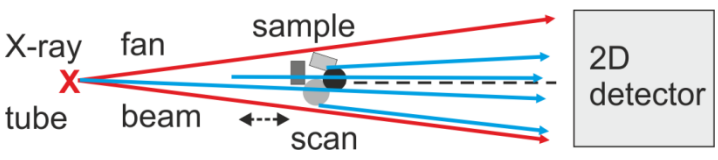

Diffraction Enhanced Imaging (DEI)	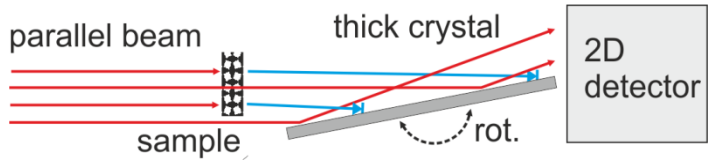
Refraction Enhanced (Dark Field) Imaging (REI)	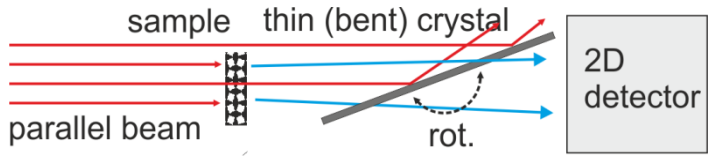
Grating Interferometry (Talbot-Lau)	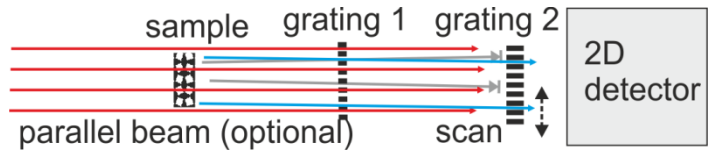

Table 2. Discrimination principles and scan parameters of X-ray refraction techniques. References listed in the two right columns, give arbitrary examples of imaging and tomographic applications.

Technique	**Discrimination**	**Scan parameter**	**Ref. imaging**	**Ref. tomography**
Pinhole Topography	pinhole	sample *x*,*y*	[Kup14a]	-
Refraction Topography	(primary) beam stop	sample *x*,*y*	[Hen87]	[Hen00] [Kup13]
Phase Contrast Radiography	propagation distance	none (distance *z*, if needed)	[Ing95] [Wil96] [Pag02]	[Zab07]
Diffraction Enhanced Imaging (DEI)	analyser crystal (reflection)	analyser angle θ	[Cha97]	[Dil00] [Mue04] [Mue09]
Refraction Enhanced Imaging (REI)	analyser crystal (transmission)	analyser angle θ (or sample *y*, if needed)	[And02] [Kup14b]	[Sun10] [Sun11]
Grating Interferometry (Talbot-Lau)	grating interference pattern	analyser grating (*x*)	[Wei05] [Pfe06] [Pfe08]	*e.g.* [Rev13] [Pfe12]

1.1 Pinhole Topography

Pinhole topography is well suited to demonstrate that X-ray refraction is a 100% scattering effect. It is a scanning technique, where the specimen is moved perpendicular to the pinhole beam. As a chief argument, this technique spares a primary beam stop in contrast to all other scattering techniques (at the expense of a very narrow incident beam). All photons, irrespective of deflected or not, are recorded by the detector. The pinhole technique is successfully applied to structures on a microscopic scale and to mesoscopic structures (powders). While in the first case a continuous displacement of the total beam is observed, the latter yields a beam broadening as function of particle size at an unchanged centre of gravity (cf. [Kup14a]).

As an example, Fig. 1 shows a reference sample of well-defined geometrical shape. The experiment was performed using a polyamide rod (diameter 1.5 mm) irradiated with 20 keV photons. The rod is moved across a 50 µm pinhole beam in 10 µm increments. The intensity is recorded by a CCD array (after conversion to visible light) of 7.2 µm pixel size 3.4 m down-stream the sample. When entering the cylinder edge, the undistorted primary beam centroid is immediately broadened and radially shifted, followed by further continuous displacement. This behaviour can be understood immediately if one recalls that the refraction angle is proportional

to the *gradient of phase shift*: since, for homogenous materials, the phase shift is proportional to the penetrated thickness, the maximum gradient of cylindrical shapes is located at the edges.

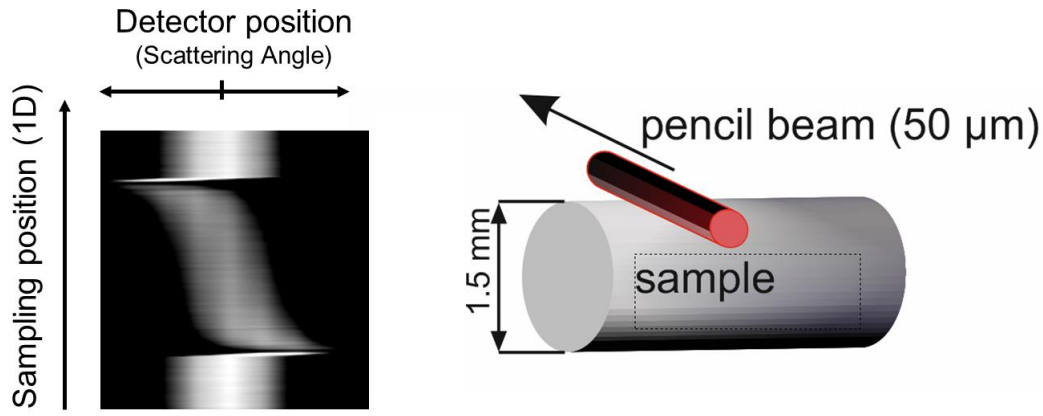

Fig. 1. Cumulative result of a 1D pinhole scan of a polymer rod. The image on the left is obtained by stacking cumulative cross sections of the (2D) images according to the 1D sampling position.

1.2 Refraction Topography

The rough sketch of the laboratory SAXS instrumentation is given in table 1 by a primary beam collimation (of Kratky type) and a beam stop in front of a single channel detector. Such kind of set-up is known to be delicate in terms of its (thermo-) mechanical stability [Hen00b]. Beyond the mentioned components, it consists of a fine structure X-ray source and a sample manipulator. For the purpose of monitoring the sample absorption and beam stability, a reference detector collects photons scattered by an inserted polymer foil in order to account for the attenuation of the refracted beam. The 2D micro scanner enables 2D imaging of specific surface distribution at a pre-selected range of scattering angle and orientation.

Beyond merely measuring the porosity by means of X-ray attenuation (radio-graphy), Fig. 2 represents the mean pore size distribution of a SiC pellet at different stages of firing. Assuming spherical pores, it is straightforward to gain the pore sizes from porosity and refraction values [Fen02]. The images clearly indicate a reduced pore size homogeneity over the whole sample after treatment at higher temperatures. The most significant difference is found at the transitional stage from the green body to the intermediate state. After this first step of densification the mean pore size varies from 0.55 µm at the outer region to a distinct concentration of 0.75 µm around the sample center. At the ceramic state the mean pore size reaches (2.1 ± 0.5) µm due to considerable pore fusion.

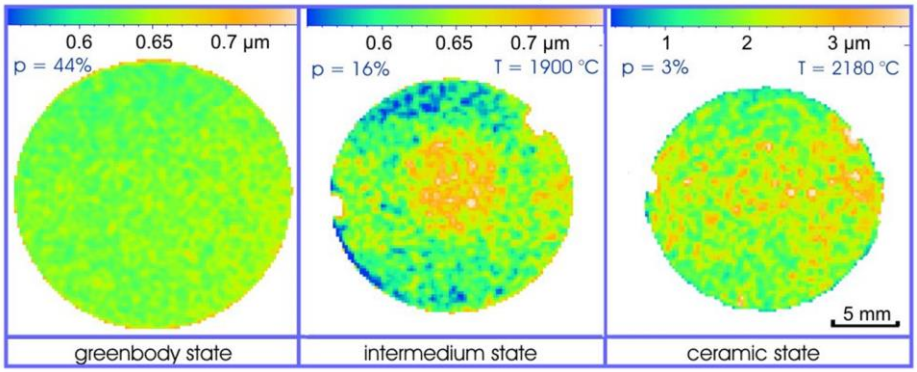

Fig. 2. Computer processed X-ray refraction topographs of a SiC pellet revealing the spatial mean pore size distribution at different stages of firing: the green body (left), an intermediate state of sintering (centre), and the fully cerammed state (right) [Hen00b]. The colour bars indicate the local pore size (averaged over the sample thickness). The porosity values, *p*, are laterally averaged.

1.3 Phase Contrast Radiography

X-ray phase contrast radiography, sometimes referred to as "propagation-based phase-contrast imaging", requires no need for additional discrimination devices if sufficiently large sample-detector distance d and detector resolution Δr are given.

It enhances the interface contrast generated by external (and internal) boundaries of weakly absorbing objects. As an advantage, it is suited for laboratory and field applications. As a disadvantage, it cannot be avoided in laboratory and field applications. It can be suppressed by the shortest possible detector distance (contact images, in the limit). In the lab scale, it is performed with rather small focal size and high detector resolution, which corresponds to the detectability of small deflection angles. Beyond the term "phase contrast" [Wil96], terms such as "pseudo holo-tomography", "Fresnel" fringes, "refraction artefacts", "edge artefacts" occur in literature. The exploitation of the enhanced edge contrast is usually not evaluated in a quantitative way. However, most efforts of numerical treatment of phase contrast imaging aim at re-establishing the pure absorption signal [Pag02, Wei11].

The discrimination effect of phase contrast imaging results from *spatial separation* of (projected) generation sites and deposition sites of refracted beam portions. Since the refraction angles θ are rather small, this can be realized in a satisfactory manner, when $d > \Delta r \,/\, \tan\theta \sim \Delta r \,/\theta$, *i.e.*, the refracted portion is deposited at least in the adjacent detector pixel. Apart from X-rays, it has been demonstrated to work for neutron imaging, as well [Str09].

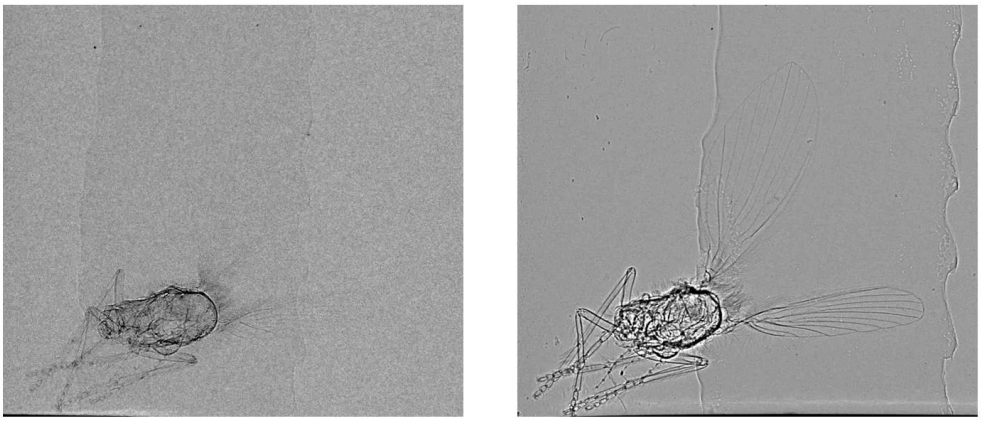

Fig. 3. Radiographs of a common fruit fly (*drosophila melanogaster*), at two different sample-detector distances of 40 mm (left) and 1755 mm (right).

1.4 Refraction Enhanced (Dark Field) Imaging (REI)

Refraction enhanced imaging employs a thin transmission crystal. The imaging effect is based on the interplay of diffraction (caused by the transmission crystal) and local violations of the (Bragg) diffraction condition (caused by refractive sample features). A 2D detector is placed in the primary beam path downstream the crystal. Since the Bragg condition causes deflection off the primary beam direction, less intensity is recorded "in the shadow" of the reflection. A refractive sample, placed upstream the crystal, modifies the incident angle on the thin crystal, which either amplifies or weakens the Bragg condition, locally.

There are several set-ups regarding the transmission crystal: a) the crystal used can be plane or bent, b) the reflection used can be operated in Laue (transmission) geometry [And02] or in Bragg (back reflection) geometry [Kup14b]. Given a homogenous, mono-

chromatic and parallel beam, a plane crystal switches to reflection mode integrally, *i.e.*, all over the illuminated region. On the other hand, a bent crystal reflects only locally, *i.e.*, it depicts the virtual rocking curve of the plane crystal, directly. Operating the crystal in the Laue geometry of diffraction the reflectivity unfortunately becomes extremely sensitive with respect to the crystal thickness [And02].

The changing intensity indicates a precise localization of the surfaces/interfaces and their relative orientation with respect to the crystal's rocking curve (Fig. 4).

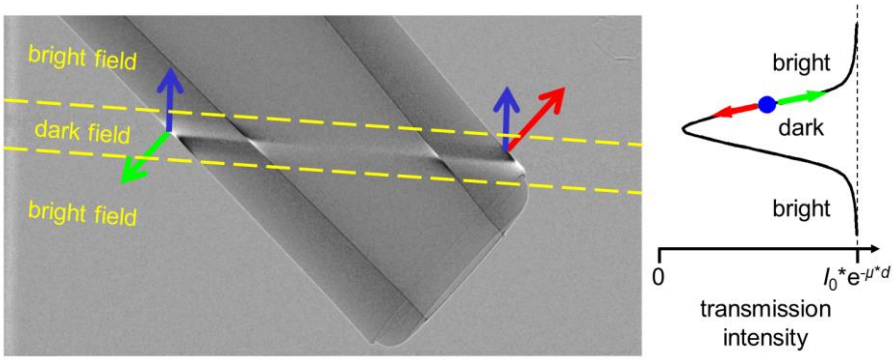

Fig. 4. Dark field radiograph (corrected for background) of the nozzle of a medical syringe [Kup14b]. Here, a bent Si (111) is operated in Bragg case at 17.4 keV. Portions of increased (green arrow) and decreased (red arrow) intensity as observed in the indicated dark field stripe are generated by refracted rays switching the crystal's Bragg condition off and on, respectively.

1.5 Diffraction Enhanced Imaging (DEI)

Diffraction Enhanced Imaging [Cha97] performs analogously to REI: the refraction induced fine tuning of a crystal's Bragg reflection. However, in contrast to REI, the image of the reflection is recorded. Given a planar (*i.e.*, not bent) crystal, a homogenous, monochromatic and parallel beam is diffracted, when the crystal is aligned properly. Ideally, without a sample, the incident beam's full cross section is reflected on a 2D detector, *i.e.*, the Bragg condition is fulfilled all over the field of view. A refractive sample deflects local beam portions, which violate the Bragg condition locally, thus reducing the intensity at those sites (Fig. 5, top).

Slightly detuning the crystal (by some seconds of arc) does not "switch off" the reflection abruptly, but yields a smooth decrease of intensity (the so-called rocking curve). Analogously to REI, in a detuned alignment the refracted beam can reconstitute the Bragg condition locally (*i.e.*, compensating the detuning), thus yielding more intensity at those sites (Fig. 5, bottom).

DEI, which could better be named "*diffraction assisted REI*", is performed by recording several images at different rocking curve positions (turning the crystal). This offers to analyse the "local rocking curves" by means of shift, broadening, and integral for each single pixel with respect to the undistorted crystal's Darwin rocking curve, thus extracting the local refractive properties.

1.6 Grating Interferometry

Grating interferometry is the common term used for the (self imaging) Talbot-Lau effect. It is a promising technique to overcome the limitations of direct refractive imaging with laboratory set-ups, as it separates the contributions of absorption (attenuation-based radiography) and refraction effects. The latter can even be separated into deflection by directed refraction of microscopic structures ("DPC" or "differential phase contrast") and phenomenologically undirected refraction by mesoscopic structures ("dark field" or Small Angle X-ray Scattering, SAXS) [Pfe12].

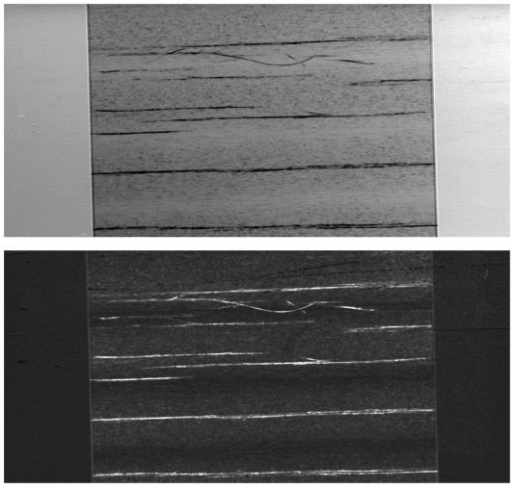

Fig. 5. Two single DEI radiographs at centre (top) and off-centre (bottom) positions of the analyser crystal, visualizing the inverted contrast generated by cracks in a CFRP sample under tensile load.

The core part of a grating interferometer is a so-called phase grating. The gridlines (of usually rectangular profile, not essential) are prepared with some µm of thickness, which corresponds to a certain phase shift (*e.g.*, π or $\pi/2$) relative to the gaps between gridlines. If irradiated with sufficiently coherent (in some cases, coherence is provided by source grating) X-rays, the modulation of the grid periodicity is recorded due to its coincidence with the diffraction period at the "Talbot distances" (or fractions).

Any kind of sample containing interfaces modifies the phase grating's interference pattern. However, it not necessary to resolve the fine structure of these patterns (in contrast to Fig. 6), as the spatial information is extracted at much lower detector resolution due to sampling the diffraction patterns by an absorptive analyser grid [Wei05] of the same periodicity.

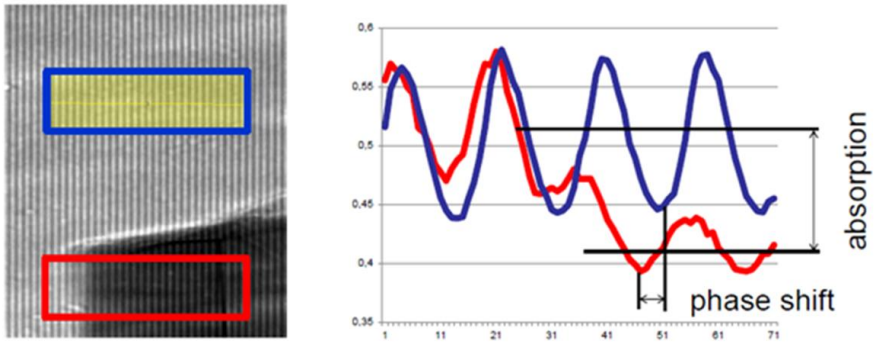

Fig. 6. High resolution radiograph of a silicon phase grating including a detail of a glass capillary (left). The profile obtained from blue box represents the interference pattern (self image) of the pure grating, which serves a reference (right). The red profile captures the transition into the capillary yielding a shift and dampening of the oscillating interference pattern (for details see [Sha16]).

2. Summary

The given survey on refractive X-ray imaging techniques refers to different levels of instrumental implementations in NDT and materials science. Refraction topography and phase contrast radiography are well suited for laboratory applications. The remaining techniques require higher coherence by parallel beam sources and monochromatic radiation at synchrotron sources. A remarkable distinction of the pinhole topography and phase contrast radiography is characterised by permitting all scattering directions while the other techniques apply a directional preselection. Table 3 comprises the suitability of the

refraction imaging techniques to laboratory or synchrotron applications as well as their tomography (CT) potentials.

Even the huge efforts in contemporary direct beam imaging techniques (radiography or absorption CT) in order to increase the image resolution will probably never reach the wavelength limit of X-ray refraction techniques.

Table 3. Classification of X-ray refraction techniques to their suitability to imaging or tomography techniques in laboratory and synchrotron scale. The entries in the scanning / imaging column stand for scanning S, direct imaging I(p) with optional variation of a parameter (see table 2).

Technique	Scanning / Imaging	Lab Imaging	Lab CT	Synch Imaging	Synch CT
Pinhole Topography	S	-	-	X	-
Refraction Topography	S	X	X	(X)	(X)
Phase Contrast Imaging	I (p)	X	X	X	X
DEI	I (p)	(-)	-	X	X
REI	I (p)	(X)	-	X	(X)
Grating Interferometry	I (p)	X	X	X	X

References

[And02] M. Ando, A. Maksimenko, H. Sugiyama, W. Pattanasiriwisawa, K. Hyodo, C. Uyama: A Simple X Ray Dark- and Bright-Field Imaging Using Achromatic Laue Optics, Japanese Journal of Applied Physics, Part 1, **41** (2002) L1016-L1018.

[Cha97] D. Chapman, W. Thomlinson, R. E. Johnston, D. Washburn, E. Pisano, N. Gmür, Z. Zhong, R. Menk, F. Arfelli, D. Sayers: Diffraction enhanced x-ray imaging, Physics in Medicine and Biology **42** (1997) 2015-2025.

[Dil00] F.A. Dilmanian, Z. Zhong, B. Ren, X.Y. Wu, L.D. Chapman, I. Orion, W.C. Thomlinson: Computed tomography of x-ray index of refraction using the diffraction enhanced imaging method, Physics in Medicine and Biology **45** (2000) 933–946.

[Fen02] F.E. Fensch-Kleemann, K.-W. Harbich, M.P. Hentschel: Microstructural Characterisation of Porous Ceramics by X-Ray Refraction Topography. cfi/Ber. DKG **79** (2002) E35- E38.

[Hen87] M.P. Hentschel, R. Hosemann, A. Lange, B. Uther, R. Brückner: Röntgenkleinwinkelbrechung an Metalldrähten, Glasfäden und hartelastischem Polypropylen, Acta Crystallographica **A 43** (1987) 506-513.

[Hen00a] M.P. Hentschel, A. Lange, B.R. Müller, J. Schors, K.-W. Harbich: X-Ray Refraction Computer-Tomography, Materialprüfung **42** (2000) 217-221.

[Hen00b] M.P. Hentschel, B.R. Müller, A. Lange, K.-W. Harbich, J. Schors, O. Wald: New development in X-Ray Topography of advanced non-metallic materials, Proc. WCNDT 15, Rome, 15.-21.10.2000.

[Ing95] V.N. Ingal, E.A. Beliaevskaya: X-ray plane-wave topography observation of the phase contrast from a non-crystalline object, J. Phys. **D 28** (1995) 2314-2317.

[Kup13] A. Kupsch, A. Lange, M.P. Hentschel, Y. Onel, T. Wolk, A. Staude, K. Ehrig, B.R. Müller, G. Bruno: Evaluating porosity in cordierite-based diesel particulate filter materials. Part 1- X-ray Refraction, Journal of Ceramic Science and Technology **4** (2013) 169-176.

[Kup14a] A. Kupsch, A. Lange, M.P. Hentschel, G. Bruno, B.R. Müller: Direct X-ray refraction of micro structures, Proc. ECNDT 11, Prague, 06.-10.10.2014.

[Kup14b] A. Kupsch, M.P. Hentschel, A. Lange, B.R. Müller: X-ray dark field imaging, Proc. ECNDT 11, Prague, 06.-10.10.2014.

[Mue04] B.R. Müller, A. Lange, M. Harwardt, M.P. Hentschel, B. Illerhaus, J. Goebbels, J. Bamberg, F. Heutling: Refraction computed tomography, MP Materials Testing **46** (2004) 314-319.

[Mue09] B.R. Müller, A. Lange, M. Harwardt and M.P. Hentschel: Synchrotron-based micro-CT and refraction-enhanced micro-CT for non-destructive materials characterisation, Advanced Engineering Materials **11** (2009) 435-440.

[Pag02] D. Paganin, S.C. Mayo, T.E. Gureyev, P.R. Miller, S.W. Wilkins: Simultaneous phase and amplitude extraction from a single defocused image of a homogeneous object, J. Microsc. **206** (2002) 33–40.

[Pfe06] F. Pfeiffer, T. Weitkamp, O. Bunk, C. David: Phase retrieval and differential phase-contrast imaging with low-brilliance X-ray sources, Nature Physics **2** (2006) 258–261.

[Pfe08] F. Pfeiffer, M. Bech, O. Bunk, P. Kraft, E.F. Eikenberry, C. Brönnimann, C. Grünzweig, C. David : Hard-X-ray dark-field imaging using a grating interferometer, Nature Materials **7** (2008) 134-137.

[Pfe12] F. Pfeiffer: Milestones and Basic Principles of Grating-Based X-ray and Neutron Phase-Contrast Imaging, International Workshop on X-ray and Neutron Phase Imaging with Gratings, AIP Conf. Proc. **1466** (2012) 2-11.

[Rev13] V. Revol, B. Plank, R. Kaufmann, J. Kastner, C. Kottler, A. Neels: Laminate fibre structure characterisation of carbon fibre-reinforced polymers by X-ray scatter dark field imaging with agrating interferometer, NDT&E International **58** (2013) 64–71.

[Sha16] Y. Shashev, A. Kupsch, A. Lange, R. Britzke, G. Bruno, B.R. Müller, M.P. Hentschel: Talbot- Lau interferometry with a non-binary phase grating for non-destructive testing, Proc. WCNDT 19, Munich, 13.-17.06.2016.

[Str09] M. Strobl, N. Kardjilov, A. Hilger, G. Kühne, G. Frei, I. Manke: High-resolution investigations of edge effects in neutron imaging, Nuclear Instruments and Methods in Physics Research **A 604** (2009) 640–645.

[Sun10] N. Sunaguchi, T. Yuasa, Q. Huo, S. Ichihara, M. Ando: X-ray refraction-contrast computed tomography images using dark-field imaging optics, Appl. Phys. Lett. **97** (2010) 153701.

[Sun11] N. Sunaguchi, T. Yuasa, Q. Huo, S. Ichihara, M. Ando: Refraction-contrast tomosynthesis imaging using dark-field imaging optics, Applied Physics Letters **99** (2011) 103704.

[Wei05] T. Weitkamp, A. Diaz, C. David, F. Pfeiffer, M. Stampanoni, P. Cloetens, E. Ziegler: X-ray phase imaging with a grating interferometer, Optics Express **13** (2005) 6296 – 6304.

[Wei11] T. Weitkamp, D. Haas, D. Wegrzynek, A. Rack: ANKAphase: software for single-distance phase retrieval from inline X-ray phase-contrast radiographs, J. Synchrotron Rad. **18** (2011) 617–629.

[Wil96] W. Wilkins, T.E. Gureyev, D. Gao, A. Pogany, A.W. Stevenson: Phase-contrast imaging using polychromatic hard X-rays, Nature **384** (1996) 335–338.

[Zab07] S. Zabler, P. Cloetens, P. Zaslansky: Fresnel-propagated submicrometer x-ray imaging of water-immersed tooth dentin, Optics Letters **32** (2007) 2987-2989.